

Traveling waves in phase-separating reactive mixtures

Tohru Okuzono* and Takao Ohta

Institute for Nonlinear Sciences and Applied Mathematics,

Graduate School of Science, Hiroshima University,

Higashi-Hiroshima 739-8526, JAPAN

Abstract

A model of phase separation of chemically reactive ternary mixtures is constructed. In this model, spatially periodic structures which coherently propagate at a constant speed emerges through a Hopf bifurcation at a finite wavenumber. It is shown by computer simulations that both lamellar and hexagonal structures undergo a coherent propagating motion in two dimensions and there are two types of traveling hexagons depending on the relative direction between the traveling velocity and the lattice vectors of the hexagonal structure. Amplitude equations for the traveling waves are derived and the stability of the traveling and standing waves are discussed.

PACS numbers: 05.45.-a, 82.40.-g, 82.40.Ck

*Present address: Yokoyama Nano-structured Liquid Crystal Project, ERATO, Japan Science and Technology Corporation, 5-9-9 Tokodai, Tsukuba 300-2635, Japan.

I. INTRODUCTION

Oscillation of spatially periodic structure appears in various systems far from equilibrium. One example is an oscillating roll structure in Rayleigh-Bénard convection of binary mixtures where a dynamical coupling between the local concentration and the local temperature causes an overshoot of domain motion resulting in an oscillation. See Ref. [1] and the earlier references cited therein. Propagation of a stripe structure has also been observed experimentally in the electro-hydrodynamic instability of liquid crystals [2]. These are the macroscopic dynamic pattern out of equilibrium.

Another example of formation of oscillating domains is microscopic. In contrast to the macroscopic non-equilibrium structures, it is emphasized here that phase transitions generally play a relevant role for dynamics of microscopic domains. It has been found that adsorbates on metal surface exhibits propagating and/or standing oscillations of nano/mesoscopic domains [3, 4]. Hildebrand et al. [5] (see also [6]) have introduced a model for traveling nanoscale stripe structures in surface chemical reactions and have successfully reproduced the traveling stripe structure. In their model, nonlocal attractive interactions between adsorbates have been considered, which cause a first order phase transition (phase separation) of the adsorbates. This property together with a chemical reaction between the adsorbates is the origin of the traveling waves.

It is worth mentioning that a traveling mesoscopic stripe pattern has also been observed experimentally in Langmuir monolayers [7]. Quite recently, this phenomenon has been studied theoretically by introducing a set of model equations, which contains a phase separation mechanism [8].

In phase separation in thermal equilibrium, domains generally grow indefinitely. However, it is well known that the domain growth ceases at a certain length scale if chemical reactions take place [9–12]. The resulting domain structure is periodic in space but not necessarily oscillatory. The mechanism for formation of periodic structures is mathematically equivalent with the microphase separation in block copolymers [13, 14].

The purpose of the present paper is to investigate, from a general point of view, self-propagation of microscopic cellular structures far from equilibrium. We consider a ternary mixture with the components A , B and C which undergo a chemical reaction $A \rightarrow B \rightarrow C \rightarrow A$. The reason for introducing this hypothetical cyclic linear reaction

is that it is the simplest way to maintain the system far-from-equilibrium and hence most convenient to explore the feature of non-equilibrium systems without being involved heavily in mathematical complication. The components A and B are assumed to be phase-separated at low temperature. This is modeled by the usual Cahn-Hilliard type equation which has been studied extensively for many years [15, 16].

Thus the new aspect of the present study is a fusion of the theory of phase transitions and physics of non-equilibrium systems. So far these two subjects have been thought of unrelated problems. Recently, however, a combined study of these different fields has been anticipated, for instance, to control various nanoscale structures.

Our main concern is the self-organized propagation not only of stripe structure but also of hexagonal structure in two dimensions. We will show in computer simulations of the present system that both a lamellar structure and a hexagonal structure exhibit coherent self-propulsion when the uniform stationary state becomes unstable.

A traveling hexagonal pattern has been obtained in the damped Kuramoto-Sivashinsky equation [17] and in a model equation for a neural field [18]. In these systems, the traveling structures appear as a secondary bifurcation after forming a motionless structure. Compared with these studies, we believe that our system of ternary reactive mixtures has a wider applicability showing that both lamellae and hexagons can travel in a self-organized manner. The preliminary results have been published in Ref. [19].

The organization of this paper is as follows. In the next section, we construct a model for phase-separating ternary reactive mixtures and perform a linear stability analysis of the model equations. In Sec. III we carry out numerical simulations of our model in one and two dimensions. It is shown that both lamellar and hexagonal structures in two dimensions can travel through a Hopf bifurcation at a finite wavenumber. In Sec. IV we derive the amplitude equations for a super-critical Hopf bifurcation from our model equations. Stabilities of traveling and standing wave solutions of the amplitude equations are analyzed and phase dynamics of the traveling lamellar structure in one and two dimensions are also developed. In Sec. V we discuss theoretically the traveling hexagonal structures considering the amplitude equations obtained by the single mode approximation. Finally, we summarize our work and touch the future problems in Sec. VI.

II. CHEMICALLY REACTIVE TERNARY MIXTURES

A. Generic model

Let us consider a ternary reactive mixture that consists of molecules of type A , B , and C and denote their local concentrations by ψ_A , ψ_B , and ψ_C , respectively. When the incompressibility condition $\psi_A + \psi_B + \psi_C = 1$ is satisfied, two of these variables are chosen to be independent. Hence we define the local kinetic variables $\psi(\mathbf{r}, t)$ and $\phi(\mathbf{r}, t)$ at position \mathbf{r} and time t as $\psi = \psi_A - \psi_B$ and $\phi = \psi_A + \psi_B$. We assume that these variables obey the following type of kinetic equations:

$$\frac{\partial \psi}{\partial t} = \nabla \cdot \left(M_1 \nabla \frac{\delta F}{\delta \psi} \right) + f(\psi, \phi), \quad (1)$$

$$\frac{\partial \phi}{\partial t} = \nabla \cdot \left(M_2 \nabla \frac{\delta F}{\delta \phi} \right) + g(\psi, \phi), \quad (2)$$

where M_1 and M_2 are the mobilities associated with ψ and ϕ and assumed to be positive constants, although they may depend on ψ and ϕ in general. F is the free energy functional of Ginzburg–Landau–type

$$F = \int d\mathbf{r} \left[\frac{D_1}{2} |\nabla \psi|^2 + \frac{D_2}{2} |\nabla \phi|^2 + w(\psi, \phi) \right], \quad (3)$$

where D_1 and D_2 are positive constants and $w(\psi, \phi)$ is a potential function. The last terms of Eqs. (1) and (2) are reaction terms and $f(\psi, \phi)$ and $g(\psi, \phi)$ are, in general, nonlinear functions of ψ and ϕ .

Kinetics of the block-copolymer systems is described by the same type equations as (1) and (2). In this case, $f(\psi, \phi)$ and $g(\psi, \phi)$, which are linear in ψ and ϕ , come from the nonlocal interaction between monomers.

Here we study the linear stability of a uniform equilibrium solution $\psi = \psi_0$ and $\phi = \phi_0$ which are determined by $f(\psi_0, \phi_0) = 0$ and $g(\psi_0, \phi_0) = 0$. Using the Fourier components ψ_q and ϕ_q with wavenumber q for the deviation of ψ and ϕ from ψ_0 and ϕ_0 , respectively, we have the linearized equations of (1) and (2) as

$$\frac{d}{dt} \begin{pmatrix} \psi_q \\ \phi_q \end{pmatrix} = \mathcal{L}_q \begin{pmatrix} \psi_q \\ \phi_q \end{pmatrix}, \quad (4)$$

where the linear evolution matrix \mathcal{L}_q is given by

$$\mathcal{L}_q = -q^2 \mathcal{M} (q^2 \mathcal{D} + \mathcal{W}) + \mathcal{A} \quad (5)$$

where \mathcal{M} and \mathcal{D} are diagonal matrices defined as $\mathcal{M} = \text{diag}(M_1, M_2)$ and $\mathcal{D} = \text{diag}(D_1, D_2)$ and $\mathcal{W} = (w_{ij})$ and $\mathcal{A} = (a_{ij})$ ($i, j = 1, 2$) are matrices with their components $w_{11} = w_{\psi\psi}(\psi_0, \phi_0)$, $w_{12} = w_{21} = w_{\psi\phi}(\psi_0, \phi_0)$, $w_{22} = w_{\phi\phi}(\psi_0, \phi_0)$, $a_{11} = f_{\psi}(\psi_0, \phi_0)$, $a_{12} = f_{\phi}(\psi_0, \phi_0)$, $a_{21} = g_{\psi}(\psi_0, \phi_0)$, and $a_{22} = g_{\phi}(\psi_0, \phi_0)$, where the functions with the subscripts ψ and ϕ mean the partial derivatives with respect to their variables. Note that the matrix \mathcal{W} is always symmetric, whereas the matrix \mathcal{A} is, in general, not symmetric although it is symmetric for the block-copolymer systems.

Eigenvalues λ_q of \mathcal{L}_q determine the linear stability of the uniform equilibrium solution. One of the control parameters for the stability in our model is the temperature T which enters through w_{11} and w_{22} as linear functions of T . Hereafter, we introduce in convenience the control parameter τ instead of T such that the uniform state becomes unstable as increasing τ . Note that \mathcal{W} determines the thermodynamic stability of the uniform state (ψ_0, ϕ_0) which is stable if $w_{11} \geq 0$ and $\det \mathcal{W} \geq 0$ in the absence of chemical reactions.

Since eigenvalues of $-q^2\mathcal{M}(q^2\mathcal{D} + \mathcal{W})$ are always real, properties of \mathcal{A} prescribe the type of instability. For simplicity, we set $M_1 = M_2 = 1$ below, which does not change the essence of the following argument. Suppose the system of ordinary differential equations for Eqs. (1) and (2) ($q = 0$ mode) is stable, that is,

$$\text{tr}\mathcal{A} < 0 \text{ and } \det \mathcal{A} > 0. \quad (6)$$

As τ is increased, the largest $\text{Re } \lambda_q$ becomes positive at a finite wavenumber $q = q_c \neq 0$ and either Turing-type ($\text{Im } \lambda_{q_c} = 0$) or Hopf-type ($\text{Im } \lambda_{q_c} \neq 0$) instabilities occur depending on \mathcal{A} . When $\det \mathcal{L}_{q_c} = 0$ and $\text{tr}\mathcal{L}_{q_c} < 0$, the Turing-type instability occurs. In this case we expect that stationary (motion-less) periodic structures emerge. On the other hand, the Hopf-type instability, which we are concerned with, occurs when $\det \mathcal{L}_{q_c} > 0$ and

$$\text{tr}\mathcal{L}_{q_c} = \frac{(\text{tr}\mathcal{W})^2}{4\text{tr}\mathcal{D}} + \text{tr}\mathcal{A} = 0 \quad (7)$$

with

$$q_c^2 = -\frac{\text{tr}\mathcal{W}}{2\text{tr}\mathcal{D}} \quad (8)$$

for $\text{tr}\mathcal{W} < 0$. In this case a traveling wave or standing oscillation are expected to reveal.

The above analysis implies that an oscillatory instability at a finite wavenumber, which is sometimes called a wave instability, is induced by the thermodynamic instability of phase separation. The wave instability occurs also in a FitzHugh-Nagumo model with nonlocal

coupling where drifting domains have been observed [20]. It should be noted that in the block copolymer systems only the Turing-type instabilities can occur since the system is variational.

B. Simplified model and its linear stability

Now we consider a specific model which show a self-propagation of spatially periodic structures. We assume that there is a strong repulsive interaction between A and B molecules, and other interactions between molecules are quite weak compared with the A - B interaction so that the potential $w(\psi, \phi)$ can be regarded as a function of ψ only. Hence, we simply put

$$w(\psi, \phi) = -\frac{\tau}{2}\psi^2 + \frac{1}{4}\psi^4, \quad (9)$$

where τ is the control parameter as mentioned in the preceding section. Furthermore we assume $M_1 = M_2 = 1$ and $D_2 = 0$. Then Eqs. (1) and (2) become

$$\frac{\partial \psi}{\partial t} = \nabla^2[-D_1 \nabla^2 \psi - \tau \psi + \psi^3] + f(\psi, \phi), \quad (10)$$

$$\frac{\partial \phi}{\partial t} = g(\psi, \phi). \quad (11)$$

Equation (10) (and (9)) is a simplified model equation. In general, the third component C may influence the interaction between A and B and, for example, the parameter τ may depend on C . However, we here ignore such an effect.

Suppose that the system undergoes the following cyclic chemical reactions:



where γ_1 , γ_2 , and γ_3 are the reaction rates. From the mass action law, the reaction terms in Eqs. (10) and (11) can be written as

$$f(\psi, \phi) = -(\gamma_1 + \frac{\gamma_2}{2})\psi - (\gamma_1 - \frac{\gamma_2}{2} + \gamma_3)\phi + \gamma_3, \quad (13)$$

$$g(\psi, \phi) = \frac{\gamma_2}{2}\psi - (\frac{\gamma_2}{2} + \gamma_3)\phi + \gamma_3. \quad (14)$$

In this case, the stationary uniform solutions ψ_0 and ϕ_0 are given by

$$\psi_0 = \frac{\gamma_3(\gamma_2 - \gamma_1)}{\gamma_1\gamma_2 + \gamma_2\gamma_3 + \gamma_3\gamma_1}, \quad (15)$$

$$\phi_0 = \frac{\gamma_3(\gamma_2 + \gamma_1)}{\gamma_1\gamma_2 + \gamma_2\gamma_3 + \gamma_3\gamma_1}, \quad (16)$$

and the matrix \mathcal{A} is given by

$$\mathcal{A} = \begin{pmatrix} -(\gamma_1 + \frac{\gamma_2}{2}) & -(\gamma_1 - \frac{\gamma_2}{2} + \gamma_3) \\ \frac{\gamma_2}{2} & -(\frac{\gamma_2}{2} + \gamma_3) \end{pmatrix}. \quad (17)$$

The Hopf-type instability occurs when

$$\gamma_1\gamma_2 + \gamma_2\gamma_3 + \gamma_3\gamma_1 - (\frac{\gamma_2}{2} + \gamma_3)(\gamma_1 + \gamma_2 + \gamma_3) > 0 \quad (18)$$

and

$$\frac{(\tau - 3\psi_0^2)^2}{4D_1} - (\gamma_1 + \gamma_2 + \gamma_3) = 0 \quad (19)$$

at $q = q_c$ where

$$q_c = \left(\frac{\tau - 3\psi_0^2}{2D_1} \right)^{1/2}. \quad (20)$$

The linear stability diagram for Eqs. (10) and (11) with Eqs. (13) and (14) in τ - γ_2 plane is shown in Fig. 1 for $D_1 = 1$, $\gamma_1 = 0.3$, and $\gamma_3 = 0.05$. The solid and dashed lines in this figure indicate the Hopf and Turing type instabilities, respectively. The stationary uniform state is stable for the parameters below these lines.

III. NUMERICAL SIMULATIONS

In this section, we shall show, in one and two dimensions, the results obtained by computer simulations of Eqs. (10) and (11) with Eqs. (13) and (14) above the stability lines in Fig. 1.

First, we confirm numerically that a propagating solution exists in one dimension. The space mesh and the time increment have been set as 0.5 and 0.001, respectively. Figure 2(a) shows such a solution for $\tau = 1.6$ and $\gamma_2 = 0.15$, which is just above the Hopf instability line (the solid line in Fig. 1). In Fig. 2 (a) the profiles of $\psi(x, t)$ (solid line) and $\phi(x, t)$ (dashed line) are plotted as functions of the spatial coordinate x at $t = 5000$. Both profiles of $\psi(x, t)$ and $\phi(x, t)$ are moving to the right, in this case, at a constant speed keeping their shapes and the phase difference between them, whereas Fig. 2 (b) depicts stationary patterns of ψ and ϕ without a phase difference for $\tau = 1.6$ and $\gamma_2 = 0.25$ above the Turing instability line.

A. Traveling lamellar pattern

Now we extend the simulations to two dimensions. The simulations have been carried out on a 128×128 square lattice with the mesh size $\Delta x = 0.5$ using the finite difference

Euler scheme with a fixed time step $\Delta t = 10^{-3}$ for several values of parameters τ and γ_2 . Other parameters are fixed at $D_1 = 1$, $\gamma_1 = 0.3$, and $\gamma_3 = 0.05$. As the initial conditions we start with homogeneous states with small random perturbations which satisfy $\langle \psi \rangle = \psi_0$ and $\langle \phi \rangle = \phi_0$ and used periodic boundary conditions, where the angle brackets mean the spatial average.

As predicted by the linear stability analysis, no pattern appears for the parameters below the solid or dashed lines in Fig. 1. For the parameters above the dashed line at which the Turing-type instability occurs, stationary lamellar or hexagonal patterns appear depending on the equilibrium values of ψ_0 and ϕ_0 . For the parameters above the Hopf-type instability line (solid line in Fig. 1), various traveling patterns are observed. Henceforth, we concentrate on the parameter region near the Hopf instability line.

Figure 3 displays three snapshots of $\psi(r, t)$, indicated in gray scale increasing from black to white, at $t = 50$ (a), 500 (b), and 5000 (c) for $\tau = 1.6$ and $\gamma_2 = 0.2$ ($\psi_0 = -0.059$, $\phi_0 = 0.29$). At the early stage irregular patterns with motions of distorted standing waves are formed [Fig. 3(a)]. After this transient regime, partially coherent lamellar structures which are traveling emerge [Fig. 3(b)]. The system eventually reaches the state in which the lamellar structure extended to the whole system is traveling at a constant speed [Fig. 3(c)]. The arrows in Fig. 3 indicate the directions of propagation of the lamellar structures. The behavior is similar to that reported by Hildebrand et al. [5] in the surface chemical reaction systems, although the evolution equations are quite different.

B. Traveling hexagonal pattern

One of the characteristic features of the present model system (10) and (11) with Eqs. (13) and (14) is that not only lamellar pattern but also hexagonal structure can undergo a coherent propagation by choosing the values ψ_0 and ϕ_0 appropriately.

Figure 4 shows one example for $\psi_0 = -0.20$, $\phi_0 = 0.40$ where three snapshots of $\psi(r, t)$ are displayed in gray scale increasing from black to white at $t = 50$ (a), 500 (b), and 5000 (c) for $\tau = 1.6$ and $\gamma_2 = 0.1$. At the early stage, droplet-like domains irregularly move accompanied with breakups and coalescence of domains [Fig. 4(a), (b)] and finally form a regular hexagonal pattern traveling in one direction at a constant speed [Fig. 4(c)]. The propagating direction of the hexagons is indicated by white arrows in Fig. 4.

Another type of traveling hexagons appears as in Fig. 5 where three snapshots of $\psi(\mathbf{r}, t)$, at $t = 50$ (a), 500 (b), and 5000 (c) are displayed for $\tau = 2.0$ and $\gamma_2 = 0.06$ ($\psi_0 = -0.33$, $\phi_0 = 0.50$). The transient behavior of this system is similar to that shown in Fig. 4. However, the propagating direction (white arrows in this figure) at the asymptotic state is perpendicular to one of the primary wave vectors.

Thus, it is found that there are at least two different types of traveling hexagons. Hereafter, we call the case shown in Fig. 4 the Type-I and in Fig. 5 the Type-II, respectively.

The several ‘phases’ of nonequilibrium states have been obtained by carrying out the simulations for various parameters. Figure 6 summarizes, in the parameter space (γ_2, τ) , the various dynamic structures in two dimensions. Each symbol indicates, respectively, stationary lamellar structure (closed squares), traveling lamellar structure (open circles), traveling hexagonal structure of Type-I (crosses), traveling hexagonal structure of Type-II (pluses), and uniform stable state (open square). For some parameters we could not distinguish between Type-I and Type-II hexagons within the present simulations. Such parameters are plotted with asterisks in Fig. 6. In this figure the Hopf and Turing instability lines are also shown for convenience, which are the same as those in Fig. 1.

It is noted here that the value of $\phi(\mathbf{r}, t)$, which is the sum of the local concentration of A and B molecules, becomes negative in some parameter region. This shortcoming is due to the simplification of the free energy given by Eq. (9). However, we have carried out the simulations avoiding this parameter region and believe that the results obtained would not be altered even when a more refined free energy is employed.

The amplitude of the traveling waves is plotted in Fig. 7 both for lamellar (open circles) and hexagonal (crosses) structures. It is evident that the bifurcation for lamellae is supercritical whereas that for hexagons is subcritical.

IV. THEORETICAL ANALYSIS OF TRAVELING LAMELLAE

The computer simulations given in the previous section show that a lamellar structure exhibits a self-organized coherent propagation above the Hopf bifurcation threshold. It should be noted that a standing oscillation has never been observed in simulations. In order to understand this property, we derive the amplitude equation at post-threshold and examine the stability of the oscillatory domains.

A. Amplitude equation

We study the time-evolution equations (10)–(14) in one dimension near the Hopf bifurcation point at the critical wavenumber q_c in a weakly nonlinear regime. The amplitude equation for Eqs. (10) and (11) near the Hopf instability line is derived by means of the usual reductive perturbation method [21, 22] assuming that the bifurcation is super-critical, which is indeed the case as has been shown in Fig. 7.

Near the bifurcation point, the most unstable mode $\mathbf{U}(x, t)$ is the relevant degrees of freedom of Eqs. (10) and (11), that is, $\mathbf{u} \sim \mathbf{u}_0 + \mathbf{U}$, where $\mathbf{u} \equiv (\psi, \phi)^T$ and $\mathbf{u}_0 \equiv (\psi_0, \phi_0)^T$. In terms of the eigen functions \mathbf{U}_L and \mathbf{U}_R defined below, the unstable mode $\mathbf{U}(x, t)$ is expressed as

$$\mathbf{U}(x, t) = W_L(x, t)\mathbf{U}_L + W_R(x, t)\mathbf{U}_R + \text{c.c.}, \quad (21)$$

where c.c. denotes the complex conjugate and $W_L(x, t)$ and $W_R(x, t)$ are the complex amplitudes of the plane wave solution propagating to the left and right, respectively. The wave number q_c and the frequency ω_c of the plane wave are determined by the eigenvalue problem:

$$(\partial_t - \mathcal{L}_{q_c})\mathbf{U}_L = 0, \quad (22)$$

where ∂_t denotes the partial differential operator with respect to t (\mathbf{U}_R also satisfies the same equation). For the present problem we choose

$$\mathbf{U}_L = \begin{pmatrix} 1 \\ \alpha \end{pmatrix} e^{iq_c x + i\omega_c t} \quad \mathbf{U}_R = \begin{pmatrix} 1 \\ \alpha \end{pmatrix} e^{-iq_c x + i\omega_c t} \quad (23)$$

with $\alpha \equiv (a_{22} + i\omega_c)/a_{12}$ and $\omega_c (> 0)$ is given by

$$\omega_c^2 = \det \mathcal{L}_{q_c} = -a_{22}^2 - a_{12}a_{21} \quad (24)$$

By the standard procedure of the perturbation [21, 22], the final amplitude equations for W_L and W_R are given, respectively, by

$$\partial_t W_L = \mu W_L + b\partial_x^2 W_L - g|W_L|^2 W_L - h|W_R|^2 W_L, \quad (25)$$

$$\partial_t W_R = \mu W_R + b\partial_x^2 W_R - g|W_R|^2 W_R - h|W_L|^2 W_R, \quad (26)$$

where all the coefficients are complex and are given by

$$\mu \equiv \frac{\tilde{\tau}}{2} q_c^2 \left(1 + \frac{ia_{22}}{\omega_c}\right), \quad (27)$$

$$b \equiv 2D_1q_c^2\left(1 + \frac{ia_{22}}{\omega_c}\right), \quad (28)$$

$$g \equiv \frac{3}{2}q_c^2\left(1 + \frac{ia_{22}}{\omega_c}\right) \left[1 + 24\psi_0^2q_c^2 \frac{a_{22} - 2i\omega_c}{9(a_{11} + a_{22})(a_{22} - 2i\omega_c) - 3\omega_c^2}\right], \quad (29)$$

$$h \equiv 3q_c^2\left(1 + \frac{ia_{22}}{\omega_c}\right) \left[1 + 24\psi_0^2q_c^2 \frac{a_{22}}{9(a_{11} + a_{22})a_{22} + \omega_c^2}\right], \quad (30)$$

and $\tilde{\tau} \equiv \tau - \tau_c$ with a critical value τ_c of τ at which the bifurcation occurs. The constant g should not be confused with the function in Eq. (14). This type of amplitude equations was also obtained in Refs. [23, 24]. Note that Eqs. (25) and (26) do not have terms proportional to $\partial_x W_L$ or $\partial_x W_R$. This reflects the fact that in our model the group velocity is always zero, that is, $d\omega(q_c)/dq = 0$, where $\omega(q) \equiv \sqrt{\det \mathcal{L}_q}$ near the bifurcation point. This comes from the particular choice of $D_2 = 0$ in Eq. (3).

B. Stability of traveling wave

Here we examine stability of the traveling wave solution of Eqs. (25) and (26). These equations have a set of solutions $W_L^{(0)}$ and $W_R^{(0)}$ as

$$W_L^{(0)} = 0, \quad W_R^{(0)} = N_0 e^{-iqx + i\Omega_0(q)t}, \quad (31)$$

where the real constants Ω_0 and N_0 are given by

$$N_0^2 = \frac{1}{g_1}(\mu_1 - b_1q^2), \quad (32)$$

$$\Omega_0 = \mu_2 - b_2q^2 - \frac{g_2}{g_1}(\mu_1 - b_1q^2), \quad (33)$$

and $\mu = \mu_1 + i\mu_2$, $b = b_1 + ib_2$ with real numbers μ_1 , μ_2 , b_1 and b_2 . A similar notation has also been utilized for g and h .

In order to study the stability of the solution (31), let us introduce deviations ξ and η as

$$W_L = W_L^{(0)} + \xi, \quad (34)$$

$$W_R = W_R^{(0)} + \eta. \quad (35)$$

Substituting Eqs. (34) and (35) into Eqs. (25) and (26) yields up to the first order of the deviations

$$\partial_t \xi = \mu \xi + b \partial_x^2 \xi - h N_0^2 \xi, \quad (36)$$

$$\partial_t \eta = \mu \eta + b \partial_x^2 \eta - (W_R^{(0)})^2 \bar{\eta} - 2g N_0^2 \eta, \quad (37)$$

where $\bar{\eta}$ is the complex conjugate to η . Setting $\xi \propto \exp(iqx + \lambda t)$, we obtain

$$\lambda = \mu - bq^2 - hN_0^2. \quad (38)$$

The growth rate of the deviation ξ is given by

$$\text{Re } \lambda = (\mu_1 - b_1q^2)\left(1 - \frac{h_1}{g_1}\right), \quad (39)$$

where we have used Eq. (32). Since $(\mu_1 - b_1q^2)/g_1 = N_0^2 > 0$, we need the stability condition for the traveling wave [23, 24]

$$h_1 > g_1. \quad (40)$$

Next, we investigate stability of the standing wave solution given by

$$W_L^{(0)} = N_0 e^{iqx + i\Omega_0 t}, \quad W_R^{(0)} = N_0 e^{-iqx + i\Omega_0 t}, \quad (41)$$

where Ω_0 and N_0 satisfy the following relation,

$$i\Omega_0 = \mu - bq^2 - gN_0^2 - hN_0^2. \quad (42)$$

We introduce the small deviations of the amplitudes $\xi(x, t)$, $\eta(x, t)$ and the phases $\varphi(x, t)$, $\theta(x, t)$ as

$$W_L = N_0(1 + \xi)e^{iqx + i\Omega_0 t + i\varphi}, \quad (43)$$

$$W_R = N_0(1 + \eta)e^{-iqx + i\Omega_0 t + i\theta}, \quad (44)$$

From Eqs. (25), (26), (43) and (44) we obtain the time evolution equations for the deviations.

The deviations of amplitudes obey up to the first order

$$\partial_t \xi = -2g_1 N_0^2 \xi - 2h_1 N_0^2 \eta + b_1 \partial_x^2 \xi - 2qb_2 \partial_x \xi - 2qb_1 \partial_x \varphi - b_2 \partial_x^2 \varphi, \quad (45)$$

$$\partial_t \eta = -2g_1 N_0^2 \eta - 2h_1 N_0^2 \xi + b_1 \partial_x^2 \eta + 2qb_2 \partial_x \eta + 2qb_1 \partial_x \theta - b_2 \partial_x^2 \theta, \quad (46)$$

where we have used Eq. (42). In the long-wave-length limit, we may retain only the first two terms of Eqs. (45) and (46). In this case, the eigenvalues of the time-evolution matrix are

$$\lambda = -2N_0^2(g_1 \pm h_1). \quad (47)$$

Since g_1 is positive when the bifurcation is super-critical, we have the stability condition of the standing wave [23, 24]

$$-g_1 < h_1 < g_1. \quad (48)$$

According to the numerical calculations based on Eqs. (29) and (30), we have not found the parameters for which the standing wave is stable as long as $g_1 > 0$. This agrees with the fact that we have never found the standing wave in the simulations of Eqs. (10)–(14).

C. Phase dynamics for traveling wave

Now we discuss phase dynamics for the traveling wave solution. We write a solution of Eqs. (25) and (26) with the deviations $\xi(x, t)$ and $\varphi(x, t)$ as

$$W_L = 0, \quad W_R = N_0(1 + \xi)e^{-iqx + i\Omega_0 t + i\varphi}. \quad (49)$$

The zeroth-order solution has been obtained in Eqs. (31). The first order equations are given by

$$\partial_t \xi = -2g_1 N_0^2 \xi + b_1 \partial_x^2 \xi + 2qb_2 \partial_x \xi + 2qb_1 \partial_x \varphi - b_2 \partial_x^2 \varphi, \quad (50)$$

$$\partial_t \varphi = -2qb_1 \partial_x \varphi + b_1 \partial_x^2 \varphi + b_2 \partial_x^2 \xi + qb_2 \partial_x \varphi - 2g_2 N_0^2 \xi. \quad (51)$$

Since the amplitude deviation decays rapidly compared with the phase deviation in the long wave-length modulation, we may eliminate ξ adiabatically by putting $\partial_t \xi = 0$ in Eq. (50) so that we have

$$\xi = \frac{1}{2g_1 N_0^2} (2qb_1 \partial_x \varphi - b_2 \partial_x^2 \varphi + 2qb_2 \partial_x \xi + b_1 \partial_x^2 \xi). \quad (52)$$

Applying Eq. (52) iteratively, we obtain the following expression of ξ as a gradient expansion of φ [23, 24],

$$\xi = \frac{qb_1}{g_1 N_0^2} \partial_x \varphi + \frac{b_2}{2g_1 N_0^2} \left(-1 + \frac{2q^2 b_1}{g_1 N_0^2} \right) \partial_x^2 \varphi + \dots \quad (53)$$

Substituting Eq. (53) into Eq. (51) we obtain up to the second-order derivatives of φ

$$\partial_t \varphi = C \partial_x \varphi + D \partial_x^2 \varphi, \quad (54)$$

where

$$C \equiv 2q \left(b_2 - \frac{g_2 b_1}{g_1} \right), \quad (55)$$

$$D \equiv \left(b_1 + \frac{g_2 b_2}{g_1} \right) \left(1 - \frac{2q^2 b_1}{g_1 N_0^2} \right). \quad (56)$$

Here we consider the case that the factor $b_1 + g_2 b_2 / g_1$ in Eq. (56) is positive so that the traveling wave solution is stable for $|q| \rightarrow 0$. In this case, the coefficient D becomes negative

for large value of $|q|$, which causes an Ekhaus-type instability. Since $1 - 2q^2b_1/(g_1N_0^2) = (\mu_1 - 3q^2b_1)/(g_1N_0^2)$, this instability occurs when

$$q^2 > \frac{\mu_1}{3b_1}. \quad (57)$$

Note that the condition $q^2 < \mu_1/b_1$ is required for the traveling wave solution to exist.

We can obtain amplitude equations for the traveling lamellar structures which are similar to the equation for the one dimensional case. The complex amplitudes $W_L(\mathbf{r}, t)$ and $W_R(\mathbf{r}, t)$ of waves propagating to the left and right in x -direction obey the following equations, corresponding to Eqs. (25) and (26),

$$\partial_t W_L = \mu W_L + b(\partial_x - \frac{i}{2q_c} \partial_y^2)^2 W_L - g|W_L|^2 W_L - h|W_R|^2 W_L, \quad (58)$$

$$\partial_t W_R = \mu W_R + b(\partial_x - \frac{i}{2q_c} \partial_y^2)^2 W_R - g|W_R|^2 W_R - h|W_L|^2 W_R, \quad (59)$$

where the coefficients μ , b , g , and h are defined in Eqs. (27)–(30).

We can also develop the phase dynamics in two dimensions from the above amplitude equation. We write a traveling wave solution of Eqs. (58) and (59) propagating to x -direction as

$$W_L = 0, \quad W_R = N_0[1 + \xi(\mathbf{r}, t)]e^{-iqx + i\Omega_0 t + i\varphi(\mathbf{r}, t)}, \quad (60)$$

where $\xi(\mathbf{r}, t)$ and $\varphi(\mathbf{r}, t)$ are the small deviations associated with the amplitude and phase, respectively. Repeating the same procedure shown above, we obtain the phase equation corresponding to Eq. (54) as

$$\partial_t \varphi = C \partial_x \varphi + D \partial_x^2 \varphi - \frac{q}{q_c} \left(b_1 + \frac{g_2}{g_1} b_2 \right) \partial_y^2 \varphi, \quad (61)$$

where C and D are given by Eqs. (55) and (56), respectively. Equation (61) implies that when $q > 0$ the phase deviation in y -direction is destabilized. This corresponds to the zig-zag-type instability.

In the numerical simulations shown in Sec. III we have never found both the Ekhaus- and the zig-zag-type instabilities. We should say that the traveling wave solution is quite stable in our model system.

V. THEORETICAL ANALYSIS OF TRAVELING HEXAGONS

In two dimensional systems, not only a lamellar structure but also a hexagonal structure are allowed to exist as a spatially periodic structure. As was shown in the previous section,

the hexagonal structure also undergoes a coherent propagation above the Hopf instability line.

We do not carry out a systematic derivation of the amplitude equations for the traveling hexagons mainly because the bifurcation is subcritical and hence evaluation of each coefficient of the amplitude equation is more involved. Here we employ a simple mode expansion focusing on the two types of the traveling pattern obtained in the simulations.

We seek a solution of Eqs. (10) and (11) in the following form, $\psi(\mathbf{r}, t) = \hat{\psi}(\mathbf{r} - \mathbf{V}t)$, $\phi(\mathbf{r}, t) = \hat{\phi}(\mathbf{r} - \mathbf{V}t)$, with a traveling velocity \mathbf{V} . Here we make the approximation that the functions $\hat{\psi}(\mathbf{r})$ and $\hat{\phi}(\mathbf{r})$ are represented in terms of the lowest Fourier modes as

$$\hat{\psi}(\mathbf{r}) = \sum_{k=-3}^3 \hat{\psi}_{\mathbf{q}_k} e^{i\mathbf{q}_k \cdot \mathbf{r}}, \quad \hat{\phi}(\mathbf{r}) = \sum_{k=-3}^3 \hat{\phi}_{\mathbf{q}_k} e^{i\mathbf{q}_k \cdot \mathbf{r}}, \quad (62)$$

where $\mathbf{q}_k \equiv (q_c \cos \frac{2\pi}{3}k, q_c \sin \frac{2\pi}{3}k)$ ($k = \pm 1, \pm 2, \pm 3$) and $\mathbf{q}_0 \equiv \mathbf{0}$. Note that $\hat{\psi}_{\mathbf{q}_0} = \psi_0$, and $\hat{\phi}_{\mathbf{q}_0} = \phi_0$. We have verified numerically that the actual spatial profile is not substantially deviated from Eq. (62) near the Hopf bifurcation line although it is subcritical.

From Eqs. (10), (11) and (62), we obtain a set of equation for $\hat{\psi}_{\mathbf{q}_k}$, $\hat{\phi}_{\mathbf{q}_k}$ and \mathbf{V} . Eliminating $\hat{\phi}_{\mathbf{q}_k}$ and introducing a real amplitude A_k and a phase θ_k as $\hat{\psi}_{\mathbf{q}_k} = A_k \exp(i\theta_k)$, we finally obtain

$$\Omega(\omega_k)A_k = \mu A_k - 3q_c^2 [2\psi_0 A_l A_m e^{-i\varphi} + A_k^3 + 2(A_l^2 + A_m^2)A_k] \quad (63)$$

for $k = 1, 2, 3$ ($l, m = k + 1, k + 2 \pmod{3}$) with

$$\Omega(\omega) \equiv \frac{\omega^2 - \omega_c^2}{\omega^2 + a_{22}^2} (a_{22} - i\omega), \quad (64)$$

where $\varphi \equiv \theta_1 + \theta_2 + \theta_3$, $\mu \equiv -q_c^2 (Dq_c^2 - \bar{\tau}) - (\gamma_1 + \gamma_2 + \gamma_3)$, $\omega_k \equiv \mathbf{q}_k \cdot \mathbf{V}$, and $\omega_c \equiv \text{Im } \lambda(q_c)$ is the critical frequency at the Hopf bifurcation point. Note that two of the three phase variables θ_k are arbitrary and only the sum φ is determined by the above equations. Therefore, Eqs. (63) and (64) under the condition $\omega_1 + \omega_2 + \omega_3 = 0$ determine A_k , φ , and \mathbf{V} .

When $A_k \neq 0$, the imaginary part of Eq. (63) gives

$$-\omega_k \frac{\omega_k^2 - \omega_c^2}{\omega_k^2 + a_{22}^2} = 6q_c^2 \psi_0 \frac{A_l A_m}{A_k} \sin \varphi. \quad (65)$$

In the special case that $\sin \varphi = 0$, Eq. (65) has solutions $\omega_k = 0$ and $\pm \omega_c$. If we choose $\omega_1 = 0$, $\omega_2 = \omega_c$, and $\omega_3 = -\omega_c$, then the traveling velocity \mathbf{V} is perpendicular to \mathbf{q}_1 [see Fig. 8(a)]. This is the Type-I solution. On the other hand, the Type-II solution of Eqs. (63) is represented as $\omega_1 = -2\omega_2$ and $\omega_2 = \omega_3$ which satisfies the condition $\omega_1 + \omega_2 + \omega_3 = 0$. In this case, \mathbf{V} is indeed parallel to \mathbf{q}_1 as shown in Fig. 8(b).

VI. CONCLUDING REMARKS

In this paper, we have constructed the model equation for phase separation of chemically reactive ternary mixtures. In this model the thermodynamic destabilization induces the Turing- or Hopf-type instability at a finite wave number depending on the parameters in the reaction terms. The phase diagram for the nonequilibrium states has been obtained numerically. Traveling waves appear as a Hopf bifurcation at a finite wavenumber. In two-dimensional simulations we have obtained the traveling lamellar structure and two types (Type-I and Type-II) of traveling hexagonal structures. The mathematical structure of these two types of traveling hexagons has been investigated by the amplitude equations derived by the single mode approximation. What we have shown in this paper is that phase transitions in a non-equilibrium condition produce a rich variety of self-organized domain dynamics which never occur in thermal equilibrium where the ordered state is motionless and is simply uniform or at most modulated in space.

We have derived the amplitude equations for the supercritical Hopf bifurcation at a finite wavenumber from the model equations and investigated the stability of the traveling wave and the standing oscillation in one-dimensional systems. The traveling wave is found to be stable in some parameter regions. However we have never found, at least numerically, any region in which the standing oscillation is stable.

There is a simple explanation as to why one needs three components of chemical species for coherently propagating domains. Suppose that the species are arrayed in one dimensional space as A, B, C, A . After one cycle of chemical reaction, this order becomes B, C, A, B . This means that domains are moving to the left. It is clear from this argument that the relative phase difference of the chemical reaction determines the propagating direction and that a standing oscillation is quite unlikely in the present system.

Thermal fluctuations have been believed to be unimportant for pattern formation far from equilibrium as long as macroscopic patterns such as Rayleigh-Bénard convection and Belousov-Zhabotinski reaction are concerned. (See, however, recent experiments [25] for electroconvection of liquid crystals.) On the contrary, when the domain structure is of microscopic scale as in the present model system, thermal fluctuations cannot be ignored near the bifurcation points out of equilibrium and might alter qualitatively the properties of the transition. Concentration fluctuations around the deterministic motion may also exhibit

some characteristic features inherent to non-equilibrium systems. We hope to return to these fundamental problems elsewhere in the future.

Acknowledgments

We would like to thank Professor A. S. Mikhailov for valuable discussions. This work was supported by the Grant-in-Aid for Scientific Research from the Ministry of Education, Science, Sports and Culture of Japan.

-
- [1] M. C. Cross and P. C. Hohenberg, *Rev. Mod. Phys.* **65**, 851 (1993).
 - [2] A. Joets and R. Ribotta, *Phys. Rev. Lett.* **60**, 2164 (1988).
 - [3] R. Imbihl and G. Ertl, *Chem. Rev.* **95**, 697 (1995).
 - [4] A. von Oertzen, H. H. Rotermund, A. S. Mikhailov and G. Ertl, *J. Phys. Chem. B* **104**, 3155 (2000).
 - [5] M. Hildebrand, A. S. Mikhailov, and G. Ertl, *Phys. Rev. Lett.* **81**, 2602 (1998).
 - [6] A. S. Mikhailov, M. Hildebrand, and G. Ertl, in *Coherent Structures in Classical Systems*, edited by M. Rubi et al. (Springer, New York, 2001) and references cited therein.
 - [7] Y. Tabe and H. Yokoyama, *Langmuir* **11**, 4609 (1995).
 - [8] R. Reigada, F. Sagués, and A. S. Mikhailov, unpublished.
 - [9] S. C. Glotzer, E. A. Di Marzio, and M. Muthukumar, *Phys. Rev. Lett.* **74**, 2034 (1995).
 - [10] J. Verdasca, P. Borckmans, and G. Dewel, *Phys. Rev. E* **52**, R4616 (1995).
 - [11] M. Motoyama and T. Ohta, *J. Phys. Soc. Jpn.*, **66**, 2715 (1997).
 - [12] Q. Tran-Cong and A. Harada, *Phys. Rev. Lett.* **76**, 1162 (1996).
 - [13] T. Ohta and K. Kawasaki, *Macromolecules* **19**, 2621 (1986).
 - [14] M. Bahiana and Y. Oono, *Phys. Rev. A* **41**, 6763 (1990).
 - [15] J. D. Gunton, M. San Miguel, and P. S. Sahni, in *Phase Transitions and Critical Phenomena*, edited by C. Domb and J. L. Lebowitz (Academic Press, New York, 1983) Vol. 8.
 - [16] A. J. Bray, *Adv. Phys.* **43**, 357 (1994).
 - [17] I. Daumont, K. Kassner, C. Misbah, and A. Valance, *Phys. Rev. E* **55**, 6902 (1997).
 - [18] C. B. Price, *Phys. Rev. E* **55**, 6698 (1997).

- [19] T. Okuzono and T. Ohta, *Phys. Rev. E* **64**, 045201 (2001).
- [20] E. M. Nicola, M. Or-Guil, W. Wolf, and M. Bär, *Phys. Rev. E* **65**, 055101 (2002).
- [21] Y. Kuramoto, *Chemical Oscillations, Waves and Turbulence* (Springer-Verlag, Berlin, 1984).
- [22] D. Walgraef, *Spatio-Temporal Pattern Formation* (Springer-Verlag, New York, 1997).
- [23] P. Coulet, S. Fauve, and E. Tirapegui, *J. Physique Lett.* **46**, L-787 (1985).
- [24] T. Ohta and K. Kawasaki, *Physica* **27D**, 21 (1987).
- [25] M. A. Scherer and G. Ahlers, *Phys. Rev. E* **65**, 051101 (2002).

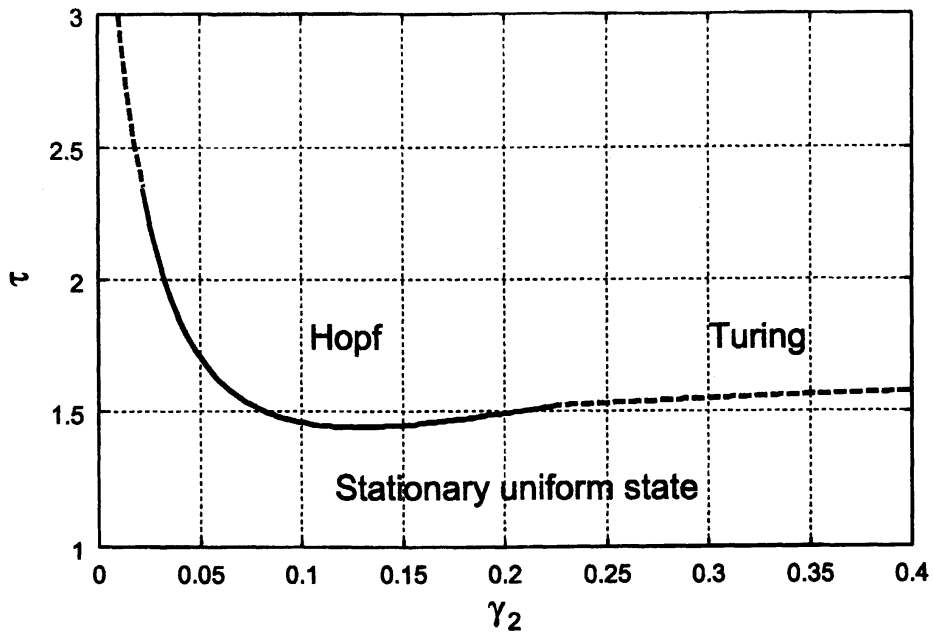


FIG. 1: Linear stability diagram for Eqs. (10) and (11) with Eqs. (13) and (14) in τ - γ_2 plane for $D_1 = 1$, $\gamma_1 = 0.3$, and $\gamma_3 = 0.05$. The solid and dashed lines in this figure indicate the Hopf and Turing type instabilities, respectively.

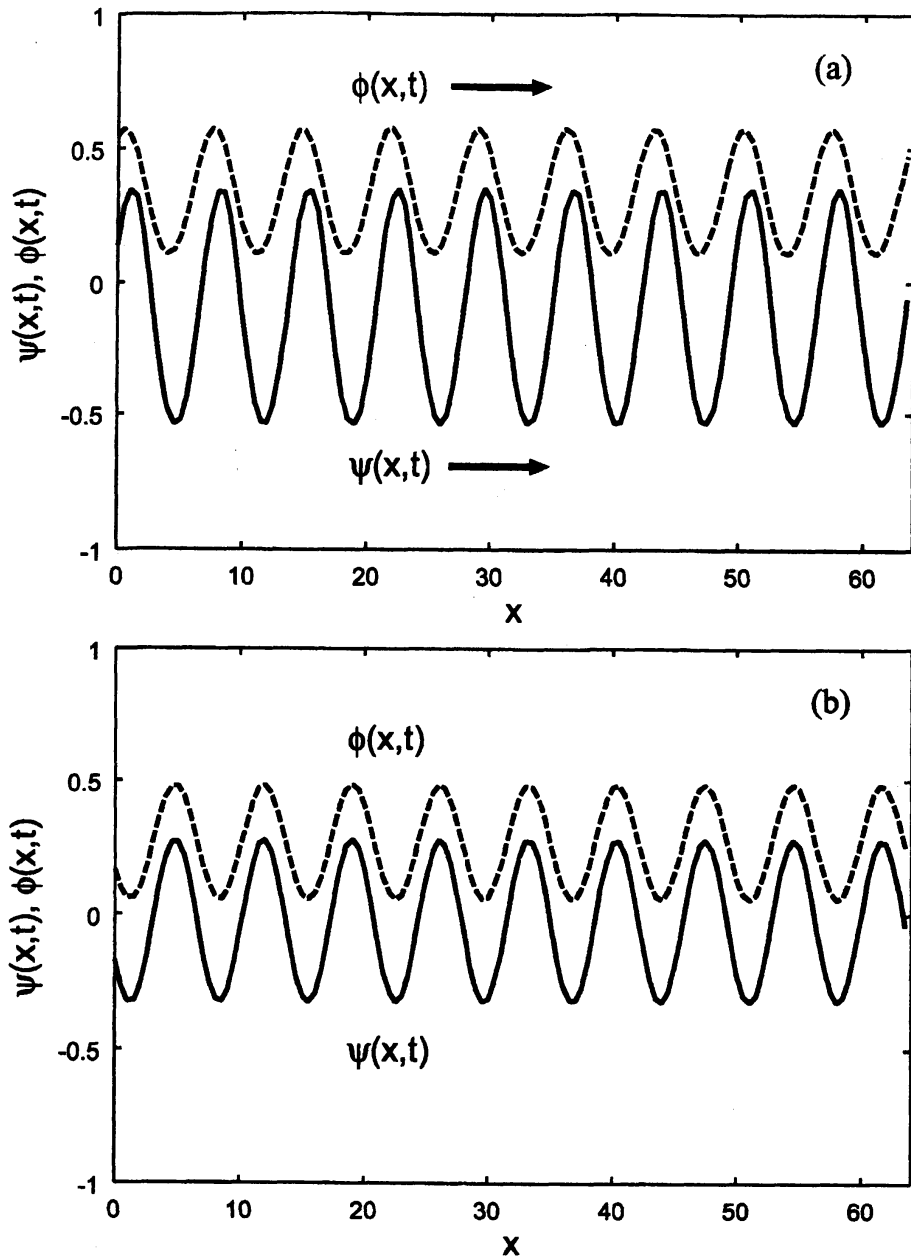


FIG. 2: Spatial profiles of $\psi(x,t)$ (solid lines) and $\phi(x,t)$ (dashed lines) obtained by one-dimensional simulations for (a) $\tau = 1.6$, $\gamma_2 = 0.15$ (just above the Hopf instability line) and (b) $\tau = 1.6$, $\gamma_2 = 0.25$ (just above the Turing instability line) at $t = 5000$. Both profiles of $\psi(x,t)$ and $\phi(x,t)$ are propagating to x -direction indicated by the arrow with the same velocity in the case of (a), whereas they are stationary in the case of (b).

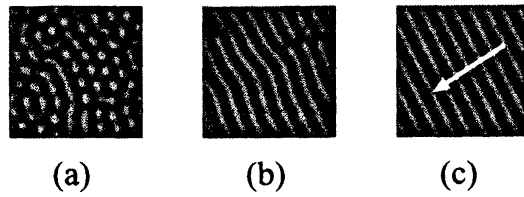


FIG. 3: Snapshots of $\psi(r, t)$, indicated in gray scale increasing from black to white, at $t = 50$ (a), 500 (b), and 5000 (c) for $\tau = 1.6$ and $\gamma_2 = 0.2$. The white arrow indicates the direction of propagation of the lamellar structure.

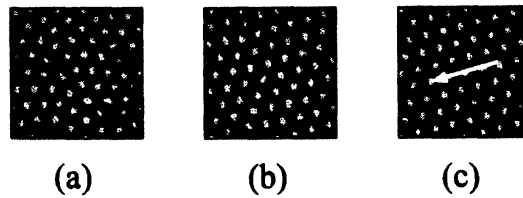


FIG. 4: Snapshots of $\psi(r, t)$ indicated in gray scale increasing from black to white at $t = 50$ (a), 500 (b), and 5000 (c) for $\tau = 1.6$ and $\gamma_2 = 0.1$. The white arrow indicates the direction of propagation of the hexagonal structure (Type-I).

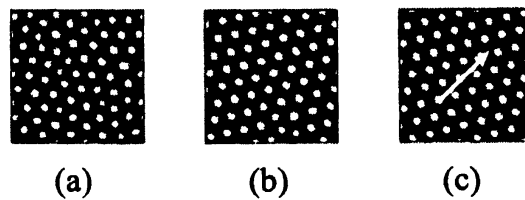


FIG. 5: Snapshots of $\psi(r, t)$ indicated in gray scale increasing from black to white at $t = 50$ (a), 500 (b), and 5000 (c) for $\tau = 2.0$ and $\gamma_2 = 0.06$. The white arrow indicates the direction of propagation of the hexagonal structure (Type-II).

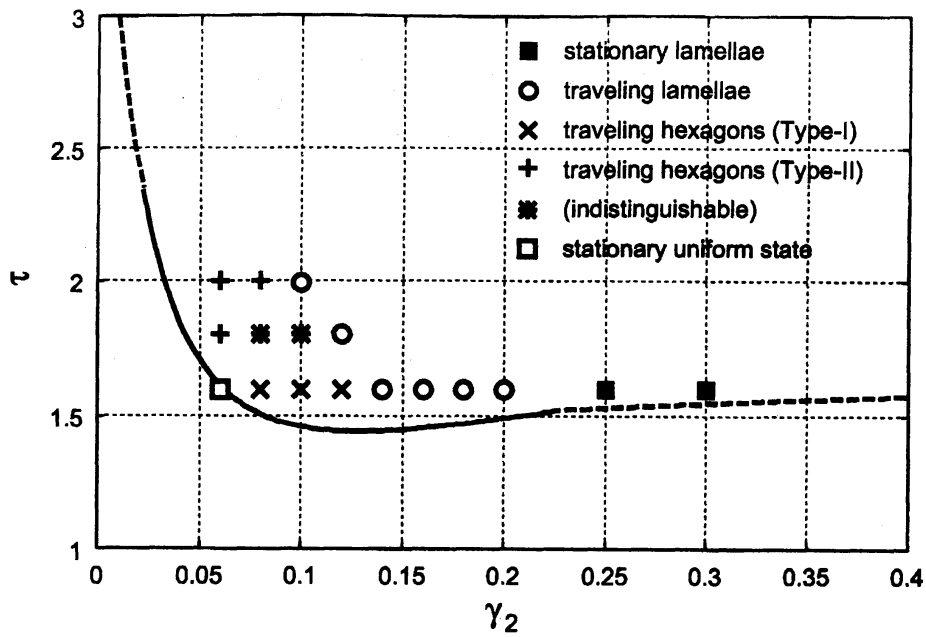


FIG. 6: Parameter dependence of the nonequilibrium states in (γ_2, τ) space. Each symbol indicates, respectively, stationary lamellar structure (closed squares), traveling lamellar structure (open circles), traveling hexagonal structure of Type-I (crosses), traveling hexagonal structure of Type-II (pluses), and stationary uniform state (open square). The asterisks mean the states that we could not distinguish between Type-I and Type-II hexagons within the present simulations. The Hopf and Turing instability lines are also shown for convenience, which are the same as those in Fig. 1.

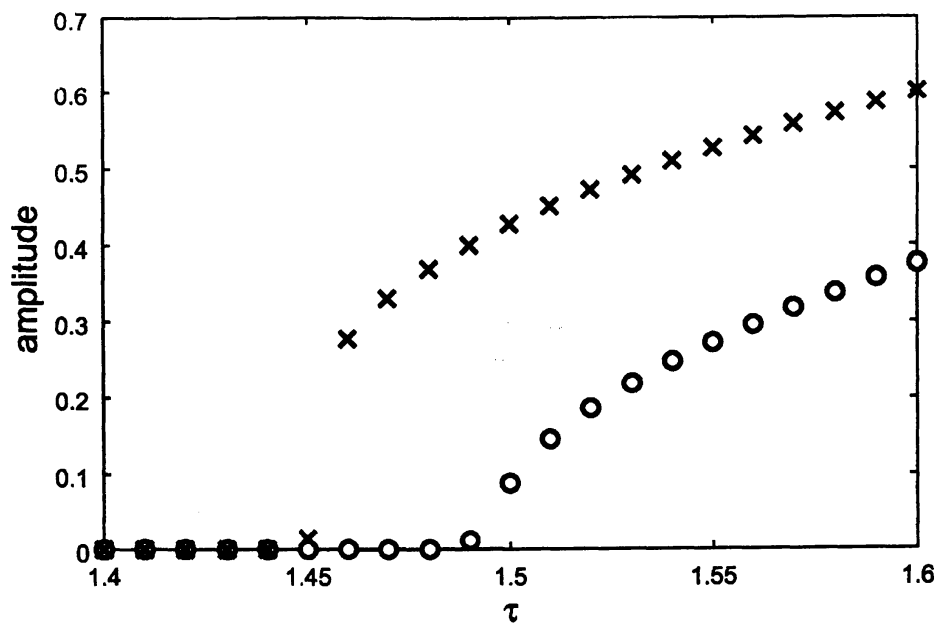


FIG. 7: Amplitudes of ψ in the traveling state for the lamellar (open circles) [$\gamma_1 = 0.3$, $\gamma_2 = 0.2$, and $\gamma_3 = 0.05$] and hexagonal (crosses) [$\gamma_1 = 0.3$, $\gamma_2 = 0.1$, and $\gamma_3 = 0.05$] structures as functions of the control parameter τ .

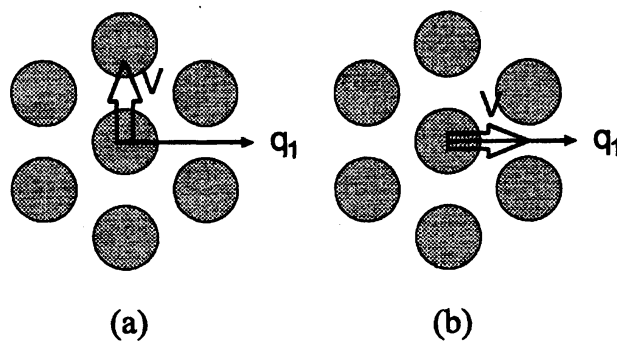


FIG. 8: Schematic picture of the directions of traveling velocity \mathbf{V} and wave vector \mathbf{q}_1 for traveling hexagonal domains of Type-I (a) and Type-II (b). Thick and thin arrows indicate the direction of \mathbf{V} and \mathbf{q}_1 , respectively, and the hatched regions represent ψ -rich domains.